

Graphene spin capacitor for magnetic field sensing

Y. G. Semenov, J. M. Zavada, and K. W. Kim

*Department of Electrical and Computer Engineering,
North Carolina State University, Raleigh, NC 27695-7911*

Abstract

An analysis of a novel magnetic field sensor based on a graphene spin capacitor is presented. The proposed device consists of graphene nanoribbons on top of an insulator material connected to a ferromagnetic source/drain. The time evolution of spin polarized electrons injected into the capacitor can be used for an accurate determination at room temperature of external magnetic fields. Assuming a spin relaxation time of 100 ns, magnetic fields on the order of ~ 10 mOe may be detected at room temperature. The observational accuracy of this device depends on the density of magnetic defects and spin relaxation time that can be achieved.

PACS numbers: 85.75.-d, 72.25.-b, 75.70.-i, 73.61.Wp

During the past two decades research in spintronic applications has focused on imitating conventional electronics based on charge transport and manipulation. A typical example is the Datta-Das spin field effect transistor,¹ which generated a wide range of variations² albeit without practical success. In general, spin transistors require (i) a long spin relaxation time τ_s compared to the spin processing time in the semiconductor channel, (ii) a sufficient spin polarization that allows discrimination between the "on" and "off" states, and (iii) stability against electronic thermal dispersion. Note that spin manipulation via the Bychkov-Rashba effect³ relies on the strength of spin-orbit coupling, which in turn is incompatible with long spin relaxation.

This Letter considers the possibility of separating the spin and charge processing in a capacitor populated with spin-polarized electrons. Robust functionality of such a spin capacitor relies on tolerance to spin injection efficiency and subsequent phase (rather than spin polarization magnitude) manipulation of spin polarization. Here we demonstrate that the state-of-art achievements in injection, detection and storage of the electron spins in a graphene based capacitor can lead to a class of spintronic devices designed for detection at room temperature of extremely weak magnetic fields.

A schematic of the proposed device is shown in Fig. 1. The device consists of graphene nanoribbons situated on top of an insulator material connected to a ferromagnetic (FM) source/drain. This structure forms a capacitor, which stores the electronic charge Q and spin under the appropriate bias V_g conditions. Operation of the spin capacitor sensor is depicted in Fig. 2. After electron injection through the FM contact a spin polarization $\mathbf{P}(t)$ is established at $t = 0$ [see Fig. 2(a)]. Unlike charge storage, $\mathbf{P}(t)$ changes in time due to spin precession in an external magnetic field and spin decoherence. As the electric bias is reversed at $t = \tau_{ex}$, the electrons leave the capacitor with rotated and reduced spin polarization so that the peak intensity I_{peak} of probe current I_{prob} through the FM contact depends on the magnitude of $P(t)$ and phase of its rotation [Fig. 2(b)]. The temporal oscillations of $\mathbf{P}(t)|_{t=\tau_{ex}}$ can be recorded by applying a series of sequential measurements with variable exposure times τ_{ex} , i.e., the duration of the electron storage in the capacitor [Fig. 2(c)]. Moreover, the iteration of such a procedure in three orthogonal device directions will supply complete information about the strength and direction of an external magnetic field.

The advantage of the proposed device consists in an easy electrical variation of spin exposure time and elimination of spin dephasing that arises in transient two-terminal schemes

involving transport. The conducting material for such a spin capacitor must possess a high electron mobility and long spin relaxation time including semiconductors with weak spin-orbital interaction. The best candidate for this application appears to be graphene nanoribbons with tunable band-gap, low spin-orbital coupling and high electron mobility.⁴

In general, $\mathbf{P}(t)$ is the difference between the ensemble-averaged spin polarization at time t [i.e., $\langle \mathbf{S} \rangle(t)$] and that of the equilibrium value $\langle \mathbf{S} \rangle_0$. Its time evolution can be described by the Bloch equation

$$\frac{d\mathbf{P}(t)}{dt} = \varpi \times \mathbf{P}(t) - \frac{\mathbf{P}(t)}{\tau_s} \quad (1)$$

with initial condition $\mathbf{P}(0) = \mathbf{P}_0$, where $\mathbf{P}_0 \parallel \mathbf{M}$ originates from spin injection from a FM contact with magnetization \mathbf{M} and τ_s is the characteristic spin relaxation time mentioned earlier. To increase the accuracy of the device, the internal magnetic field \mathbf{H}_{in} due to the magnetic parts of the device must be incorporated into consideration along with the external contribution \mathbf{H}_{ex} .⁵ Thus, the electron spin precession vector is given by $\varpi = \gamma_e \mathbf{H}$, where $\mathbf{H} = \mathbf{H}_{in} + \mathbf{H}_{ex}$ and γ_e is the electron gyromagnetic ratio. For simplicity, we assume that magnetic fields are not too strong to require distinguishing between longitudinal and transversal spin relaxation times. Then the solution of Eq. (1) reads

$$\mathbf{P}(t) = P_0 e^{-t/\tau_s} \left\{ \mathbf{p} \cos \omega t + 2\mathbf{n}(\mathbf{n} \cdot \mathbf{p}) \sin^2 \frac{\omega t}{2} + (\mathbf{n} \times \mathbf{p}) \sin \omega t \right\}, \quad (2)$$

where $P_0 = |\mathbf{P}_0|$, $\mathbf{p} = \mathbf{P}_0/P_0$, $\omega = |\varpi|$, and $\mathbf{n} = \varpi/\omega = \mathbf{H}/H$. The spin-dependent output signal from the FM contact is given as $I_{peak}(t) \propto \mathbf{P}(t) \cdot \mathbf{p}$ in terms of variable exposure time $t = \tau_{ex}$.

Once $I_{peak}(t)$ is measured in the manner discussed above, the Fourier transformation $F(f) = \int_0^\infty I_{peak}(t) \cos(ft) dt$ can be found as

$$F(f) = \tau_s P_0^2 \left(\frac{\cos^2 \alpha}{1 + x^2} + \frac{(1 + x^2 + y^2) \sin^2 \alpha}{[1 + (x + y)^2][1 + (x - y)^2]} \right), \quad (3)$$

where $x = \tau_s f$, $y = \tau_s \omega$, and α is the angle between \mathbf{p} and \mathbf{n} . In the case of $\alpha = \pi/2$ (i.e., the magnetic field is perpendicular to the injected spin polarization \mathbf{P}_0) at $f = 0$ (the dc component), Eq. (3) reproduces the Hanle effect: $F(0) = \tau_s P_0^2 / (1 + \omega^2 \tau_s^2)$,⁶ which can be applied to the determination of prefactor of Eq. (3) and relaxation time τ_s . More importantly, $F(f)$ possesses a pronounced peak at ω provided $1/\tau_s \ll \omega$ and the angle α is not close to zero. Then the peak position f_p immediately indicates the strength of the total

magnetic field $H = f_p/\gamma_e$. Note that this treatment does not involve determination of the peak intensity making the sensor insensitive to spin injection efficiency.

In the case of non-negligible $1/\tau_s\omega$ or slight deviation \mathbf{H} from the direction of spin polarization \mathbf{P}_0 (small α), the peak of $F(f)$ can be masked and shifted from the resonant frequency ω by the first term in Eq. (3). To mitigate these effects, the signal processing can be modified by subtracting $2\tau_s P_0^2/(1+x^2)$ from $F(f)$. This procedure defines a new function $\Phi(f) = 2\tau_s P_0^2 \phi_S(x, y) \sin^2 \alpha$, where $\phi_S(x, y)$ takes the form of the expression in brackets of Eq. (3) after substitutions $\cos^2 \alpha \rightarrow -1$ and $\sin^2 \alpha \rightarrow 1$. Even though the peak position f_p of $\Phi(f) [\sim \phi_S(x, y)]$ is now no longer dependent on α , it is still subject to deviation from the desired answer (i.e., ω) as $1/\tau_s \approx \omega$ in Fig. 3. Analysis indicates that this error can be corrected by equation

$$\omega\tau_s = y = x_p - \frac{b}{6x_p + x_p^3}, \quad (4)$$

which holds with high precision for $f_p\tau_s \equiv x_p \gtrsim 1$ and $b = 2.5$. Thus, Eqs. (3) and (4) coupled with function $\Phi(f)$ establish the basis for the spin capacitor application to magnetic field measurement.

In order to determine the external field \mathbf{H}_{ex} , measurement of \mathbf{H} (or, more practically, ω via f_p) must be completed in at least three different orientations of the device, e.g., along the X, Y and Z axes. Apparently, repositioning the device does not alter the contribution of $\mathbf{H}_{in} = (H_X^{(in)}, H_Y^{(in)}, H_Z^{(in)})$ but results in permutation of \mathbf{H}_{ex} components as

$$\begin{aligned} \mathbf{H}^{(1)} &= (H_X^{(ex)}, H_Y^{(ex)}, H_Z^{(ex)}), \\ \mathbf{H}^{(2)} &= (-H_Y^{(ex)}, H_X^{(ex)}, H_Z^{(ex)}), \\ \mathbf{H}^{(3)} &= (H_X^{(ex)}, -H_Z^{(ex)}, H_Y^{(ex)}). \end{aligned} \quad (5)$$

Solutions y_k of Eq. (4) for resonant frequencies $\omega_k = y_k/\tau_s$ that correspond to the different device orientations $k = 1, 2, 3$ (i.e., three equations) yield all three components of \mathbf{H}_{ex} (three unknowns) assuming that $H_j^{(in)}$ are known parameters of the device:

$$\gamma_e^2 \sum_{j=X,Y,Z} \left(H_j^{(in)} + H_j^{(k)} \right)^2 = \omega_k^2. \quad (6)$$

An important characteristic of the device is its detection sensitivity, which is closely related to the accuracy ε of measurement of the peak position f_p for $\Phi(f)$. Limiting the measurement error Δf_p to a fraction of the intrinsic broadening ($1/\tau_s$) of the Fourier transformed

signal, $\Delta f_p \tau_s = \gamma_e \Delta H \tau_s \approx \varepsilon \ll 1$. For example, $\varepsilon \sim 1\%$ leads to $\Delta H \sim 5 \times 10^{-10}(\text{Oe})/\tau_s(\text{s})$. This estimate shows that the relaxation time τ_s is a crucial parameter, which limits the applicability of the device. Consequently, the spin relaxation time τ_s of electrons needs to be evaluated.

The most important mechanism at room temperature appears to be electron decoherence due to irregular interactions with localized spin moments as the electron thermally fluctuates between localized states.⁷ For electron localization in graphene nanoribbons in particular, magnetic defects such as the ribbon edges or carbon vacancies could be responsible for spin relaxation. Taking into account uncertainties of the interaction strength and density of defects, we can evaluate the relaxation time τ_s in a quantitative manner.

It has been shown that the fluctuation in local field $\hbar\mathbf{\Omega}(t)$ with characteristic time τ_p can be responsible for electron spin relaxation rate $\tau_s^{-1} = \frac{1}{2} \langle \mathbf{\Omega}^2(t) \rangle \tau_p$.^{7,8} We estimate $\langle \mathbf{\Omega}^2(t) \rangle$ assuming that phonon mediated transitions within energy spectrum ε_ν of nanoribbon confinement potential produce fluctuations of electron densities $|\Psi_\nu(r_i)|^2$ at the N magnetic moments located at lattice sites $r_i = (x_i, z_i)$, $i = 1, \dots, N$. We also assume that the corresponding electron wave functions $\Psi_\nu(x, z) = \psi_\nu(z)\phi_0(x)$ can be factorized into longitudinal $\psi_\nu(z)$ and transversal $\phi_0(x)$ parts, where $\phi_0(x)$ is bounded by ribbon width d . For such electron states, the effective field induced by magnetic defects with spins \mathbf{I}_i takes the form in energy units

$$\hbar\mathbf{\Omega}_\nu = J a_0 \sum_i |\psi_\nu(z_i)|^2 |\phi_0(x_i)|^2 \mathbf{I}_i, \quad (7)$$

where J is the exchange interaction constant of the magnetic defect and a_0 is the area of graphene unit cell. At room temperature, a weak magnetic field cannot polarize the localized spins so that a thermal averaging yields $\langle \mathbf{I}_i \rangle = 0$ and $\langle \mathbf{\Omega}_\nu \rangle = 0$. On the other hand, the random dispersion of non-correlated \mathbf{I}_i leads to the finite mean square result

$$\langle \mathbf{\Omega}_\nu^2 \rangle = \frac{J^2 a_0^2}{\hbar^2} \sum_i |\psi_\nu(z_i)|^4 |\phi_0(x_i)|^4 I(I+1). \quad (8)$$

Electron thermal fluctuations among the different states ν leads to dispersion of the spin precession $\langle \mathbf{\Omega}^2 \rangle = \sum_\nu \langle \mathbf{\Omega}_\nu^2 \rangle P_\nu$, where $P_\nu = e^{-\varepsilon_\nu/k_B T} / \sum_\nu e^{-\varepsilon_\nu/k_B T}$. Applying the eigenfunctions $\psi_\nu(z)$ for the confined potential and summing over N localized spins by integrating with a linear density n_1 , one can find a mean-square estimate. In the simplest case of a strong confinement for a range $L \gg d$ along nanoribbon imposes $\varepsilon_\nu - \varepsilon_d = \pi^2 \hbar^2 \nu^2 / 2m^* L^2$

with $\nu = 1, 2, \dots$ and $m^* = \pi\hbar/v_F d$. Here, ε_d is the energy of transversal confinement. Under the condition that $\varepsilon_1 \ll k_B T \ll \varepsilon_d$, averaging of Eq.(8) over ν can be approximated with

$$\langle \Omega^2 \rangle = \frac{9}{4\pi} \frac{J^2 a^2 n_1}{\hbar^2 d^2 L} I(I+1) \ln \frac{2mL^2 k_B T}{\pi^2 \hbar^2}. \quad (9)$$

The two-level model in Ref. (7) predicts slowing of spin relaxation in the limit of high temperatures due to a dynamical averaging effect. However, the rate of spin relaxation in a multilevel system slightly increases with temperature. Using typical parameters for graphene $J = 0.1$ eV, $I = 1/2$, $\tau_p = 1$ ps and for nanoribbons with dimensions, $d = 20$ nm and $L = 1$ μ m, Eq. (9) leads to a spin relaxation time estimate of $\tau_s \simeq 100$ ns provided the density of non-compensated spins is $n_1 \simeq 10^6$ cm⁻¹. For this case, the graphene spin capacitor can determine magnetic fields as low as 10 mOe at room temperature assuming measurement uncertainty ε of a few percent.

In the limiting case of zero magnetic impurity concentration, the weak hyperfine interaction with ¹³C (interaction constant of approximately -44 MHz)⁹ leads long spin relaxation times $\tau_s \gg 1$ s. Another mechanism due to surface irregularities, adapted to electron diffusion over a discrete energy spectrum,¹⁰ predicts more realistic values of $\tau_s \sim 100$ μ s. Thus purification of graphene nanoribbons can enhance the room temperature sensitivity of the spin capacitor device to a few μ Oe.

In summary, a concept for a magnetic sensing spintronic device is proposed, based on spin phase measurements of a graphene spin capacitor that provides greater sensitivity at room temperature than conventional magnetic sensors.¹¹ In addition, this device is expected to possess excellent scalability and can be easily integrated to the current electronics technology.

This work was supported in part by the US Army Research Office, NSF, and the FCRP Center on Functional Engineered Nano Architectonics (FENA).

-
- ¹ S. Datta and B. Das, Appl. Phys. Lett. **56**, 665 (1990).
- ² I. Žutić, J. Fabian, and S. Das Sarma, Rev. Mod. Phys. **76**, 323 (2004).
- ³ Y. A. Bychkov and E. I. Rashba, Pis'ma Zh. Eksp. Teor. Fiz. **39**, 66 (1984) [JETP Lett. **39**, 78 (1984)]; J. Phys. C **17**, 6039 (1984).
- ⁴ A. H. Castro Neto, F. Guinea, N. M. R. Peres, K. S. Novoselov, and A. K. Geim, Rev. Mod. Phys. **81**, 109 (2009).
- ⁵ The effect of \mathbf{H}_{in} on spin precession in the channel (Fig. 1) may be negated, at least in part, by applying a subsidiary magnet with magnetization compensating that in the FM source/drain.
- ⁶ M. I. Dyakonov and V. I. Perel, in *Optical Orientation*, edited by F. Meier and B. P. Zakharchenya (Elsevier, Amsterdam, 1984), p. 11.
- ⁷ Y. G. Semenov and K. W. Kim, Phys. Rev. Lett. **92**, 026601 (2004); Phys. Rev. B **75**, 195342 (2007).
- ⁸ B. I. Shklovskii, Phys. Rev. B **73**, 193201 (2006).
- ⁹ O. V. Yazyev, Nano Lett. **8**, 1011 (2008).
- ¹⁰ D. Huertas-Hernando, F. Guinea, and A. Brataas, Eur. Phys. J. Special Topics **148**, 177, (2007).
- ¹¹ M. P. Ledbetter, I. M. Savukov, V. M. Acosta, D. Budker, and M. V. Romalis, Phys. Rev. A **77**, 033408 (2008).

Figure captions

Fig. 1. (Color Online) Schematic view of the spin capacitor magnetic sensor which consists of graphene nanoribbons on top of an insulator material connected to a ferromagnetic source/drain with magnetization vector \mathbf{M} . Under an applied bias, polarized electrons are injection into the capacitor and their spins precess around the vector sum \mathbf{H} of external \mathbf{H}_{ex} and internal \mathbf{H}_{in} magnetic fields. The gate voltage pulses V_g control electron expose time τ_{ex} . The current response I_{prob} is used to determine \mathbf{H}_{ex} .

Fig. 2. Diagram of (a) the applied voltage pulses $V_g(t)$ and (b) current response $I_{prob}(t)$ upon a reverse pulse. The peak amplitude I_{peak} is phase-specific such that it is maximal for spin polarization parallel to \mathbf{M} , and minimal for opposite spin phase. (c) Oscillations of I_{peak} that are recorded after a series of measurements at different τ_{ex} . The frequency determines the strength of the total magnetic field. The spin relaxation time leads to damping of the oscillations.

Fig. 3. Function $\phi_S(x, y)$ plotted at different y ($=\tau_s\omega$). The dashed vertical lines indicate the maximum of each curve (i.e., $x_p = f_p\tau_s$). As $1/y$ becomes non-negligible, f_p deviates from the resonant frequencies $y/\tau_s = \gamma_e H$ requiring the use of Eq. (4).

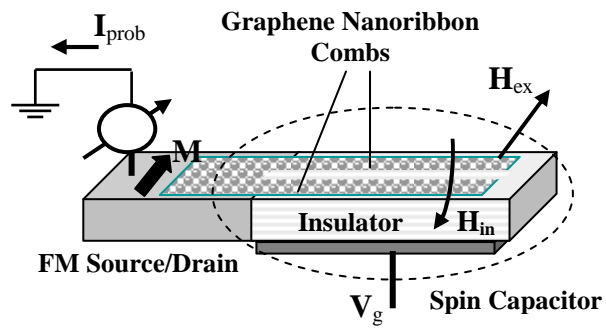


Fig. 1: Semenov et al.

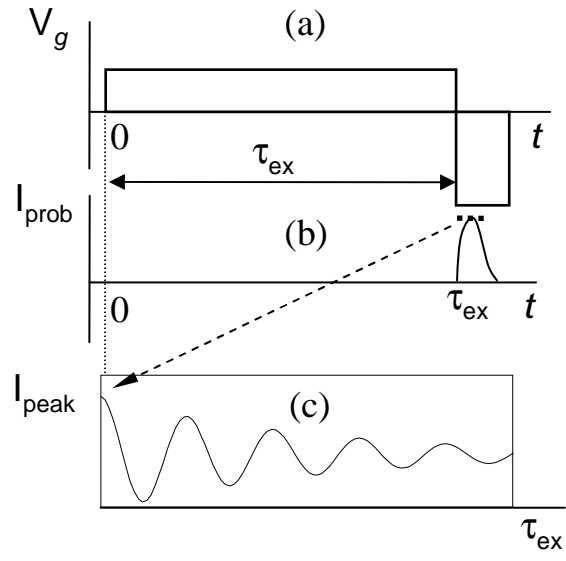


Fig. 2: Semenov et al.

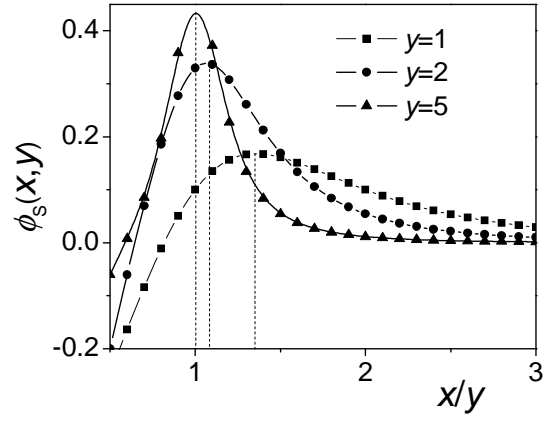


Fig. 3: Semenov et al.